R. & M. No. 3078
(17,946)
A.R.C. Technical Report

MINISTRY OF SUPPLY

AERONAUTICAL RESEARCH COUNCIL
REPORTS AND MEMORANDA

Low-Speed-Tunnel Model Tests on the Flow Structure Behind a Delta-Wing Aircraft and a 40 deg Swept-Wing Aircraft at High Incidences

By
D. A. KIRBY and A. SPENCE

LONDON: HER MAJESTY'S STATIONERY OFFICE
1958
PRICE 8s. 6d. NET

Low-Speed-Tunnel Model Tests on the Flow Structure Behind a Delta-Wing Aircraft and a 40 deg Swept-Wing Aircraft at High Incidences

By

D. A. Kirby and A. Spence

Communicated by the Director-General of Scientific Research (Air)
Ministry of Supply

Reports and Memoranda No. 3078*

April, 1955

Summary.—In view of the possibility of trimming some swept-wing aircraft at incidences above the stall, there has been a desire to visualise the whole pattern of vortex sheets and separated flow starting from the stalling wing, and to follow it back beyond the tailplane. To supplement other methods, a swivelling head has been used, giving the velocity, pitch and yaw, and results are given in this report for a 48-deg delta (*Javelin*) and a 40-deg swept-wing aircraft (*Swift* without fences).

The tests showed that at incidences beyond the stall there is a large bubble of separated flow behind the wing. For the delta at 35 deg this bubble had not closed at the station of the tailplane and extended over the whole of the region behind the wing.

The velocity and pressure field found in the separated flow resembles that behind a square plate at 90 deg. The vorticity pattern, measured in a plane cutting the bubble of separated flow from the stalled wings, is complicated by rotating masses of air inside the bubbles, between the strong inner vortex sheets, and the weaker tip vortices.

The results have been analysed to show the effect of change of tail height.

1. *Introduction.*—In view of the possibility of trimming some swept-wing aircraft at incidences above the stall, there has been a desire to visualise the whole pattern of vortex sheets and separated flow starting from the stalling wing, and to follow it back beyond the tailplane. To supplement other methods a swivelling head has been used, giving the velocity, pitch and yaw; results are given in this report for a delta and a 40-deg swept-wing aircraft (i.e., *Javelin* and *Swift* without fences (*see* Figs. 1 and 2)).

The present method is crude in that the swivelling head is stabilized by fins which are behind the pitch and static holes, so that the results in rapidly changing flow patterns will not be exact. The instrument does, however, give a numerical answer which is good enough to allow the effect of changes in tailplane height to be calculated.

Various devices (fences, notches, etc.) have been used successfully to remove pitching instability near the stall from swept wings without tailplane or with a low tailplane. Such devices are often of little use with a high tailplane, and a method of observing the effect of fences, etc., on the flow near the tailplane may be of value.

The present report gives the flow measurements for the two models without stall delaying devices or flaps.

* R.A.E. Tech. Note Aero. 2361, received 21st October, 1955.

2. *Method.*—The tests were made in the No. 1, $11\frac{1}{2}$-ft Low-Speed Tunnel at the Royal Aircraft Establishment between April and July, 1954. The *Javelin* model had a scale of 1/11th and the *Swift* model a scale of 1/8th. Both models were hung on a light strut rig. The tunnel speed was 120 ft/sec for the bulk of the tests, giving Reynolds numbers of $1 \cdot 2 \times 10^6$ for the *Javelin* and $0 \cdot 9 \times 10^6$ for the *Swift*, based on the mean chord of the wing. The tunnel speed was reduced to 80 ft/sec for the tests with the *Javelin* wing at 50-deg incidence.

2.1. *Instrument* (Fig. 3).—The measuring instrument consisted of a small pitot-static-tube, fitted with four vanes and mounted so that it was free to set itself in the local stream direction both in pitch and in yaw. The rotation about the pitch axis was obtained by mounting the instrument on cone bearings, angles of $\pm$ 70 deg to the horizontal being permitted by the holder. The holder was fixed to the top of a long rod carried in standard ball-races to allow a complete yaw range (Fig. 3). The rod was telescopic so that a range of height was available, but the locking chucks could not be tightened from outside the tunnel. It is proposed that the instrument should be modified for future tests so that the height of the instrument could be altered whilst the tunnel is running.

Measurements of the pitot and static pressures were made with an inclined manometer. The downwash angle was measured by sighting on the pitot-static-tube with a telescope, and the yaw angle obtained from a pointer attached to the telescopic rod and moving over a drum fitted to the main casing. The instrument corrections were determined from measurements made with no model in the tunnel.

There was about $2\frac{1}{2}$ in. between the static holes and the centre of pressure of the vanes (it is hoped that this can be reduced for future tests). It has been convenient to assume that the measured values of downwash, yaw and velocity apply at the pivot point of the instrument.

The velocities have not been corrected for blockage. The downwash angle has been corrected for the small tunnel-constraint correction.

The accuracy of reading for steady conditions was between $\pm \frac{1}{2}$ deg and $\pm$ 1 deg for the downwash and between $\pm$ 1 deg and $\pm$ 2 deg for the yaw angle. With very low velocities and high angles of yaw the accuracy would be $\pm$ 5 deg for the worst conditions.

2.2. *Tests Made.*—In the preliminary tests, circular traverses A were made with the instrument attached to the tunnel-floor turntable. The interpretation of these traverses proved difficult and a cross-tunnel traverse (C) was made for the later tests on the delta wing. Traverse C coincided with traverse A at the tailplane position (Fig. 1). For all traverses the spacing of the grid is given in Figs. 1 and 2; parts of the tunnel structure prevented an even spacing along traverse C.

Measurements of the pitot pressure, static pressure, downwash and yaw angles were made at four incidences for both models. The lift and pitching moments of the two models are shown in Figs. 10 and 12. The incidences were chosen as follows:

(*a*)	Near the beginning of the pitch instability	= 15 deg
(*b*)	Where the instability is large	= 20 deg
(*c*)	Where the lateral instability was most pronounced[1,2]	= 24 deg for swept-wing = 27 deg for delta wing
(*d*)	Where the stall is fully developed	= 35 deg.

In addition a few measurements were made at traverse C for the delta wing at 50-deg incidence.

The titanium-oxide technique[3] was used to study the flow in the upper-surface boundary layer for both wings at incidences up to 35 deg.

3. *Presentation of Results.*—The observed values of pitot pressure, static pressure, and the downwash and yaw angles have been analysed to give the three components of velocity, V_x, V_y and V_z. The component of vorticity having its axis along the free-stream direction has been evaluated as $(\bar{c}/V_0)\{(\Delta V_z/\Delta_y) - (\Delta V_y/\Delta_z)\}$, the sense being chosen so that the ordinary trailing vorticity is positive. The value is taken as that at the centre of a rectangle of sides Δy, Δz and has been calculated for all the small rectangles in the grid. Thus, four values of V_z and of V_y are used in calculating each value of vorticity. If the errors in all these velocities were additive the maximum error in vorticity would be $0 \cdot 5$.

The basic data for traverse C behind the delta wing is given in Fig. 5, where contour lines have been drawn for the static pressure (C_p) and the longitudinal velocity (V_x), and where the transverse velocities are shown in magnitude and direction*. The downwash and vorticity at traverse C and the vorticity for traverse A are shown in Fig. 6. The boundary where the total head in the wake reaches the free-stream value is shown on the static pressure and vorticity pictures for traverse C.

Contour lines have been drawn in Fig. 9 for the longitudinal velocity, downwash and vorticity at traverse A behind the 40-deg swept wing.

The horizontal projection of the wing, body, and the tailplane of the *Javelin* or *Swift* is shown on each illustration in Figs. 5, 6 and 9. For the two lower incidences, mean values of the longitudinal velocity and downwash over the tailplane are given in the figures.

Sketches of the flow patterns obtained on the upper surface are given in Figs. 4 and 8.

4. *Flow Behind the Delta Wing.*—4.1. *Velocity and Static Pressure.*—The titanium-oxide tests of the flow in the boundary layer (Fig. 4) show that the stall starts near the wing tip and spreads inwards with increase of incidence, until at about 20 deg, the breakdown of the flow at the leading edge has almost reached the body. At 20 deg the flow has completely separated over the outer part of the wing.

Longitudinal velocity contours are given in Fig. 5 in a vertical plane $0 \cdot 4$ semi-spans behind the wing trailing edge (traverse C). There is a small region of low velocity behind the wing tip at $\alpha = 15$ deg. With increase of incidence this region grows, until, at 27 deg, the air is flowing against the direction of the main stream. The separated flow on the wing has extended into the wake as a ' bubble ' which will close downstream of the wing.

The bubble behind a round plate at 90-deg incidence can be defined as bounded by circles through which the mean velocity in the free-stream direction is zero. A similar definition can be applied approximately to the asymmetric bubbles behind the outer wings of the delta. For instance, at $\alpha = 35$ deg the bubble defined as above would stretch to a positive-velocity contour line of about $0 \cdot 5$. Regions of negative velocity are shown on the figures by dots (Figs. 5 and 6). The bubbles increase in size, until at 50 deg a negative velocity band at the level of the wing trailing edge unites the two main regions of separated flow behind the wings. The bubbles behind the outer wings rise a little as they go back from the wing, and there is an upwash in this area. There is a large downwash nearer the centre of the wing, and full velocity air is carried down behind the body.

Some idea of the extent of the bubble in the downstream direction is given at $0 \cdot 75$ semi-span in Fig. 7, where the zero velocity contour is constructed by joining the leading and trailing edge of the wing to the points of zero velocity from traverses A and C. The end of the bubble will coincide with the end of the zero velocity contour, though the bubble will be wider than the zero velocity contour between the wing and the end.

* *Note:* The difference in height between the positions of the velocities measured for the straight traverse C and for the curved traverse A is because of the different pivot axes about which the model was rotated (*see* Fig. 1).

The length of the bubble increases with incidence; and, when measured from the wing leading edge, is about 4 times the local $c \sin \alpha$.

Since the sections in Fig. 7 are at $0 \cdot 75$ of the semi-span, they do not pass through the centre of the bubbles, particularly at the higher incidences, where the bubble centre is nearer $0 \cdot 5$ semi-span. At $\alpha = 35$ deg, the traverse C will cut the central axis of the bubble near its maximum section.

Fig. 5 shows the boundary of the wake. Considering again $\alpha = 35$ deg, this boundary coincides with a longitudinal velocity of $1 \cdot 2 V_0$, and a static pressure of about $- 0 \cdot 4q$. All the central part of the bubble at traverse C has a static pressure of about $- 0 \cdot 75q$. Outside this central region of uniform suction, there are signs of a ring of still lower pressure ($- 0 \cdot 8$ to $- 0 \cdot 85q$) before the pressure begins to rise.

In Ref. 4, the flow behind a square (or round) plate at 90 deg is given, and if a section through the maximum diameter of the bubble is constructed, the resulting diagram shows marked similarity to the traverse described above behind the swept wing. The maximum velocity is again $1 \cdot 2 V_0$, and the static pressure $- 0 \cdot 4q$ at the edge of the wake. The central suction is $- 0 \cdot 7q$, and there is a slight further reduction in pressure outside this region before the pressure rises again. If the projected height of the wing chord is used as corresponding to the side of the plate, the bubble is somewhat longer on the swept wing than on the plate.

The static pressure behind the 90-deg plate gets more negative with distance from the plate up to about half-way along the bubble, behind which the mixing process begins to close the bubble, and the pressure rises again. Traverse C on the delta wing passes near the middle of the bubbles at 35-deg and 50-deg incidences, and the suction has increased between traverses A and C, A being nearer to the wing.

4.2. *Vorticity and Downwash.*—The vorticity diagrams (Fig. 6) and the surface flow (Fig. 4) show the inboard movement of a vortex sheet as the tip stalls (though this is more clearly seen in Fig. 9 for the swept wing, in which case the regions of separated flow are smaller, and do not so much distort the picture). At the larger incidences for the delta wing, large regions of vorticity are shown inside the separated flow bubbles where the longitudinal velocity is negative, so that rotating air is carried towards the wing. Reference to Fig. 6, 27-deg incidence, will show that at traverse A (nearer to the wing) a sheet of vorticity appears along the upper edge of the bubble, together with the main sheet separating it from the wing root and body. At traverse C (further from the wing), the upper edge-layer has disappeared and the bubble air is now rotating. In addition to the inner vortex sheet and the rotating air inside the bubble, there is also a small tip vortex outside the bubble.

A traverse is needed further back where the bubble has closed in order to tell to what extent mixing removes any rotation from the wake. The present data gives a lead on this point, since traverse A cuts the bubble while traverse C is behind it for the one case of $\alpha = 20$ deg in Fig. 6. In traverse A there is a vorticity level of 3 in the bubble, with a negative vorticity region of $- 2$ below it. By traverse C the positive vorticity is reduced to 1 and the negative band to $- \frac{1}{2}$. This suggests that at greater distances behind the wing, the inboard vortex sheets and a small pair of tip vortices will form the persistent vortex pattern.

Negative vorticity regions are found above and below the rotating bubbles, appearing as long strips. These may be connected with the laminar instability for a swept wing[5] which leads to a series of negative vortices in the outer part of the boundary layer of the unstalled wing. If this layer is separated and becomes the boundary of the bubble, it is possible that the negative vorticity may persist longer than if it is on the wing surface, in which latter case it causes early transition. This point needs further study.

5. *Flow Behind the 40-deg Swept Wing.*—The contour lines of the longitudinal velocity, downwash and vorticity are plotted in Fig. 9, and the flow patterns on the wing sketched in

Fig. 8. The inboard spread of the negative velocity region was less marked on the swept wing than on the delta (Figs. 5 and 9). At 35-deg incidence the region of reversed flow (shown by dots in Fig. 9) extended inboard as far as 45 per cent of the semi-span on traverse A, instead of over almost the whole of the wing, as on the delta. The static pressure distributions were similar to those obtained for the delta wing and are not reproduced in this report.

The vorticity diagrams show the inward movement of the main vortex sheet inboard of the bubble, with a small tip vortex outside the bubble. The titanium-oxide test at $\alpha = 15$ deg showed signs of a tip vortex as well as showing the starting point of the inboard vortex sheet.

The downwash at the tailplane position was less for the swept wing than for the delta. The tailplane arm is longer for the swept wing model.

6. *Effects in the Neighbourhood of the Tailplane.*—6.1. *Delta Wing.*—The values of longitudinal velocity and downwash in the tailplane region have been analysed to find the effect of tailplane height on the pitching moment. Since there is only one traverse, a constant tail arm has been considered for the various tail heights*. The tailplane contribution to pitching moment has been calculated by multiplying the mean of the local values of $(V_x/V_0 \cos \varepsilon)^2 \times (\alpha - \varepsilon)$, taken over each tailplane region, by $dC_m/d\eta_T$, measured on the balance at low wing incidence. The balance measurements were made for the highest tailplane position (i.e., *Javelin*) and are given in Table 2. The tailplane contribution, obtained by this method, has then been added to the measured moments without tailplane to give the values plotted in Fig. 11. The moments are not shown for the two lowest tailplane positions at $\alpha = 35$ deg since the local downwash is zero and the tailplane will have stalled.

Fig. 6 shows that the *Javelin* tailplane is in a region of high downwash for incidences greater than 15 deg. Between 15 deg and 27 deg the downwash at the tailplane is increasing at a greater rate than the incidence, and the tailplane is destabilizing (Fig. 10). Above 27 deg the value of $d\varepsilon/d\alpha$ falls, and the mean velocity over the tailplane is reduced, but the downwash remains larger than the incidence so that the tailplane at zero angle gives a nose-up moment (Fig. 10). By 35 deg the average velocity over the tailplane has become very small.

Fig. 11 shows that lowering the tailplane to 40 per cent of its original height above the wing chord would remove nearly all the pitching instability. There would also be a gain in tailplane power at the higher incidences. The tailplane powers shown in Fig. 11 are based on the mean local velocity and apply to the unstalled tailplane.

6.2. 40-*deg Swept Wing.*—Similar calculations were made for the swept wing for incidences of 15 deg, 20 deg and 24 deg. The agreement with balance measurements is good for 15 deg and 20 deg, but poor at $\alpha = 24$ deg when the tailplane tip has stalled (Fig. 12).

Although the *Swift* tailplane is below the highest downwash for all four incidences, it is still in a part of the wake where the downwash is increasing rapidly with incidence. There is therefore a pitching instability when there are no fences (Fig. 12).

The pitching moments have also been calculated for a lower tailplane position. It is assumed that the middle of the net semi-span has been lowered $2\frac{1}{2}$ ft full-scale and that there is no dihedral. With this tailplane the pitching instability near the stall is eliminated (Fig. 12).

7. *Conclusions.*—7.1. *Instrumentation.*—The present system gives a general picture of the flow behind the wings, but with the size of the swivelling pitot used, the results cannot be accurate in regions of rapid flow change. The present scheme is being modified to give more easy traversing, and to use a more compact pitot.

* *Note:* The traverse strictly applies to only one line in the tailplane; the position of this line relative to the tailplane leading edge varying with incidence and tailplane height.

A new 5-tube instrument is being made, of Conrad type[6], with a central pitot. A null method of reading will be used to determine the flow direction by electrical control of the angular settings of the head from outside the tunnel.

7.2. *Flow Behind Stalled Delta Wing.*—A better picture is being formed of the mixed flow behind a stalled wing when there are bubbles of separated flow attached to the outer wings, lying between an inner vortex sheet separating the bubble from the unstalled wing and body, and a small tip vortex. In a traverse through these regions of separated flow, the flow pattern is complicated by the movements inside the bubble. If the bubble is defined by contours in x, z planes such that there is no mean longitudinal velocity through them, then the general picture of motion inside the bubble is of a reversed longitudinal flow towards the wing up the core of the bubble, returning round the outside, together with rotation of all or part of the bubble in the direction of the lift vorticity. Further work is needed to find the flow pattern further back, where the bubbles have closed. It is expected that the persistent vortex regions will consist of the inner vortex sheets, and the smaller tip vortices, and that the mixing, which closes the bubble, will have broken up the vorticity in the wake. It is possible that the flow inside the bubble might be neglected if the boundary is represented by a vortex sheet of suitable strength distribution, but a simpler case than the swept wing would be chosen if any theory is to be developed.

7.3. *Flow at Tailplane.*—The tailplane effect is governed both by the variation of downwash with incidence, and by its position relative to a low velocity wake. This method allows the interplay of these factors to be seen, and helps an appreciation of the possibilities of improving the longitudinal stability and tail effectiveness by movements of the tailplane.

NOTATION

V_0	Free-stream velocity
q	Free-stream dynamic head $= \frac{1}{2}\rho V_0^2$
V_x, V_y, V_z	Components of velocity along rectangular axes; x-axis is in direction of free stream and V_x is positive when in direction of the free stream
ε deg	Downwash angle defined as the acute angle between the horizontal and the local flow direction, measured in a plane parallel to the plane of symmetry; positive when the local flow is downwards irrespective of the sense of V_x
C_p	Local static-pressure coefficient relative to free-stream static pressure

REFERENCES

No.	*Author*	*Title, etc.*
1	J. F. Holford and F. W. Dee ..	Low-Speed-Tunnel tests on the Gloster *Javelin* at incidences above the stall. R.A.E. Tech. Note Aero. 2263. A.R.C. 16,332. September, 1953.
2	D. A. Kirby	Low-Speed-Tunnel tests on the Supermarine *Swift* at incidences above the stall. R.A.E. Paper (Unpublished).
3	A. B. Haines	Some notes on the flow patterns observed over various swept-back wings at low Mach number (in the R.A.E. 10-ft $\times$ 7-ft High Speed Tunnel). R.A.E. Tech. Note Aero. 2330. A.R.C. 17,067. September, 1954.
4	R. A. Fail, T. B. Owen and R. C. W. Eyre	Preliminary Low-Speed Wind-Tunnel tests on flat plates and airbrakes: flow, vibration and balance measurements. C.P. 251. January, 1955.
5	P. R. Owen and D. G. Randall ..	Boundary-layer transition on a swept-back wing—A further investigation. R.A.E. Paper (Unpublished).
6	G. G. Brebner	Boundary-layer measurements on a 59-deg swept-back wing at low speed. C.P. 86. August, 1950.

TABLE 1

Details of Models

	Javelin 1/11th scale	*Swift* 1/8th scale
WING		
Area: S	7·66 sq ft	4·78 sq ft
Span: b	4·73 ft	4·04 ft
Mean chord: $\bar{c} = S/b$	1·62 ft	1·18 ft
Aspect Ratio: A	2·92	3·43
Thickness/chord ratio centre-line	10 per cent	9·5 per cent
Thickness/chord ratio kink	10 per cent	10 per cent
Thickness/chord ratio tip	7 per cent	10 per cent
Chord at centre-line	2·88 ft	1·90 ft
Chord at kink	1·39 ft	1·11 ft
Chord at tip	0·49 ft	0·66 ft
Distance of kink from centre-line	1·36 ft	1·02 ft
=	0·575 semi-spans	0·505 semi-spans
Dihedral	0 deg	2 deg
Wing-body angle	0 deg	$2\frac{1}{2}$ deg
TAILPLANE		
Gross area (projected): S_T	0·94 sq ft	0·97 sq ft
Span: b_T	1·55 ft	1·61 ft
Mean chord $\bar{c}_T = S_T/b_T$	0·610 ft	0·60 ft
Thickness/chord ratio	9 per cent	9 per cent
Tailplane setting for balance measurements	0 deg	− 3 deg
Dihedral	0 deg	10 deg
Tailplane arm (c.g. to near quarter-chord point): l_T	1·92 ft	1·98 ft
Tailplane volume coefficient: $\bar{V} = S_T l_T/(S\bar{c})$	0·146	0·339
C.G. POSITION		
Aft of leading-edge centre-line chord	1·55 ft	1·24 ft
Below fuselage datum	0 ft	0·05 ft

TABLE 2

Lift, Drag and Pitching Moment for Javelin (*Flaps* 0 *deg*)

α (deg)	C_L	C_D	C_m	$\frac{\partial C_m}{\partial \eta_T}$
No tailplane				
0·25	0·006	0·0147	+ 0·0030	
5·4	0·294	0·0261	0·0063	
10·55	0·564	0·0649	0·0042	
15·65	0·762	0·1633	+ 0·0009	
18·2	0·821	0·2330	− 0·0004	
20·7	0·861	0·3081	− 0·0037	
23·2	0·866	0·3617	− 0·0086	
25·7	0·862	0·4203	− 0·0239	
28·2	0·824	0·4643	− 0·0293	
30·7	0·823	0·5114	− 0·0250	
35·7	0·820	0·6069	− 0·0267	
$\eta_T = 0$ deg, $\eta = 0$ deg				
0·25	0·001	0·0160	+ 0·0072	
5·4	0·296	0·0271	− 0·0064	
10·55	0·585	0·0689	− 0·0260	
15·65	0·790	0·1714	− 0·0358	
18·2	0·843	0·2331	− 0·0312	
20·7	0·876	0·3021	− 0·0183	
25·7	0·835	0·4139	0	
30·7	0·781	0·4852	− 0·0004	
35·7	0·795	0·5937	− 0·0146	
$\eta_T = -6\frac{1}{2}$ deg, $\eta = 0$ deg				
5·4	0·261	0·0265	+ 0·0326	− 0·00600
20·7	0·846	0·2946	0·0178	− 0·00555
25·7	0·822	0·4072	0·0242	− 0·00372
30·7	0·779	0·4868	+ 0·0074	− 0·00120
35·7	0·795	0·5965	− 0·0090	− 0·00086

Note: The coefficients in Tables 2 and 3 have not been corrected for the wake blockages since the correction for the pitot readings is unknown.

TABLE 3

Lift, Drag and Pitching Moment for Swift (*no fences*) (*Flaps* 0 *deg*)

α (deg)	C_L	C_D	C_m	$\dfrac{\partial C_m}{\partial \eta}$
No tailplane				
0	− 0·007	0·0209	− 0·0131	
7·1	+ 0·365	0·0371	+ 0·0074	
12·2	0·631	0·0957	0·0139	
17·25	0·835	0·2072	0·0226	
19·8	0·861	0·2700	0·0317	
22·3	0·871	0·3350	0·0317	
23·75	0·828	0·3572	0·0352	
24·75	0·795	0·3731	0·0264	
25·75	0·788	0·3905	0·0234	
27·25	0·805	0·4266	0·0234	
29·75	0·824	0·4762	0·0244	
32·3	0·845	0·5366	0·0211	
37·3	+ 0·865	0·6558	+ 0·0045	
$\eta_T = -3$ deg, $\eta = 0$ deg				
0	− 0·038	0·0232	+ 0·0252	
7·1	+ 0·367	0·0389	− 0·0017	
12·2	0·655	0·1061	− 0·0177	
14·75	0·753	0·1582	− 0·0145	
17·25	0·838	0·2128	− 0·0055	
19·8	0·863	0·2731	+ 0·0135	
21·3	0·869	0·3099	0·0168	
22·3	0·866	0·3352	+ 0·0183	
24·75	0·826	0·3801	− 0·0207	
27·25	0·863	0·4456	− 0·0679	
29·75	0·913	0·5131	− 0·1057	
32·3	0·953	0·5894	− 0·1443	
37·3	+ 1·015	0·7087	− 0·1989	
$\eta_T = -3$ deg, $\eta = 8$ deg				
0	0·002	0·0234	− 0·0373	0·00782
7·1	0·413	0·0428	− 0·0673	0·00820
12·2	0·689	0·1120	− 0·0819	0·00803
17·25	0·862	0·2231	− 0·0608	0·00691
22·3	0·888	0·3455	− 0·0261	0·00555

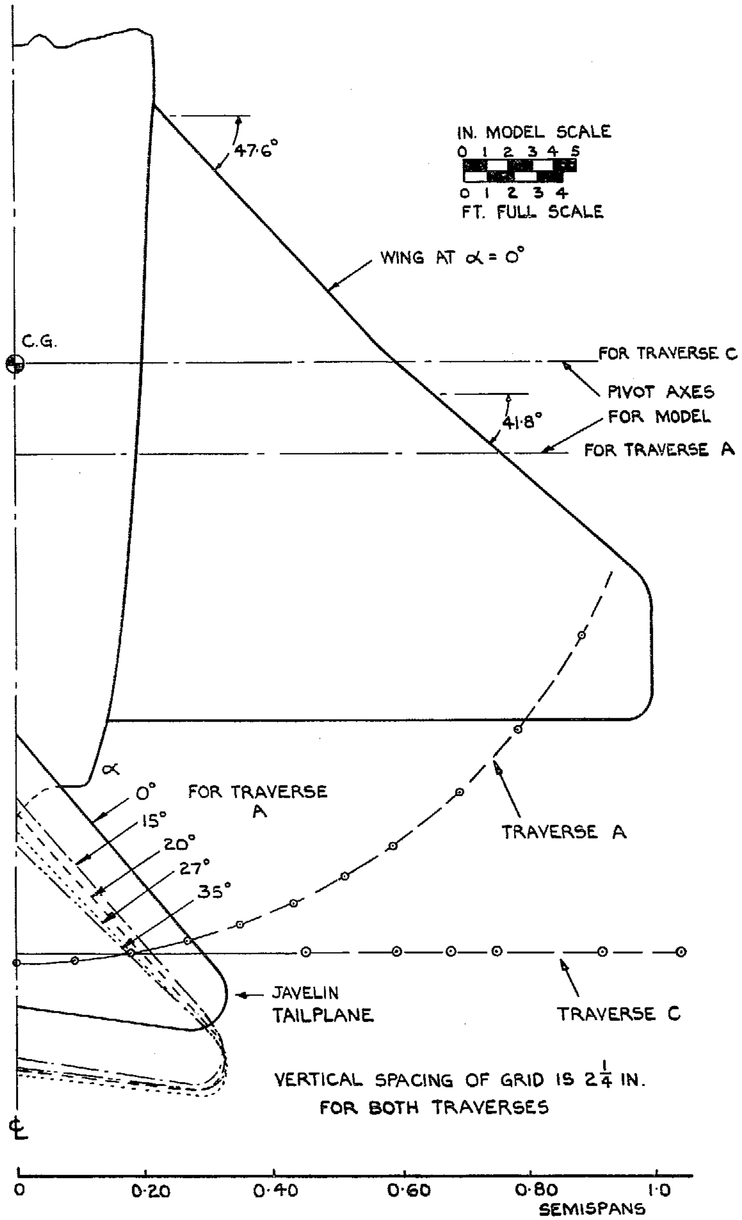

FIG. 1. Plan view of delta wing.

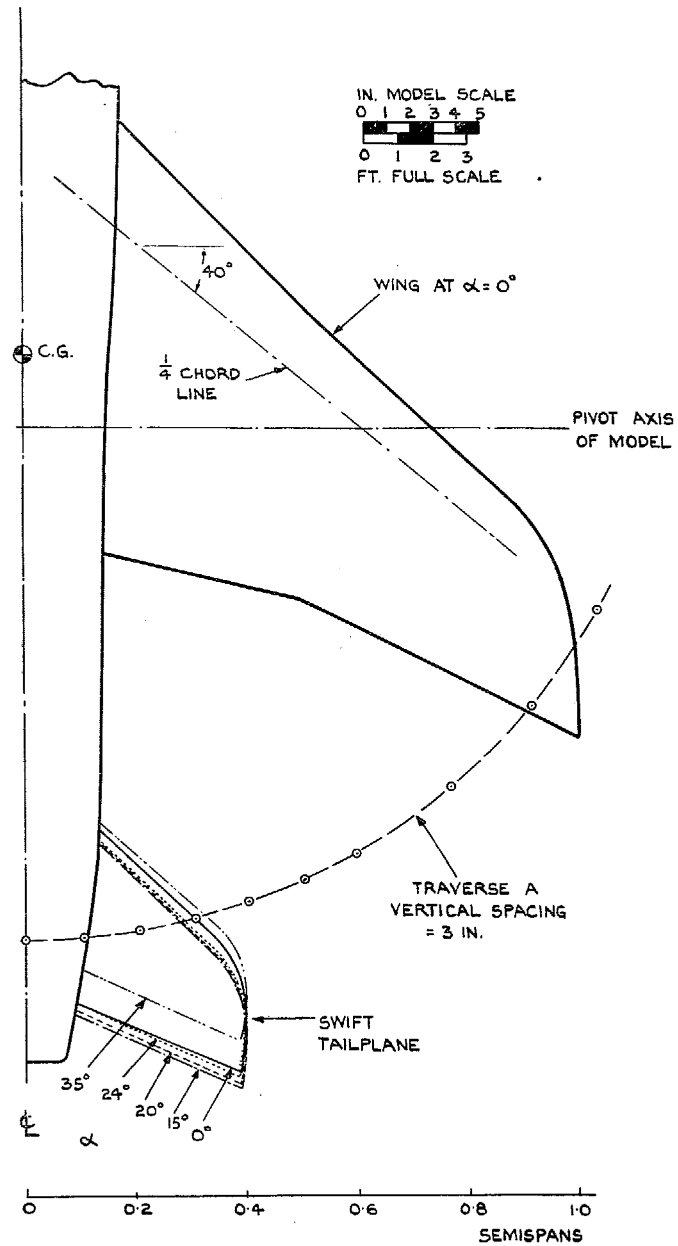

FIG. 2. Plan view of 40-deg swept wing.

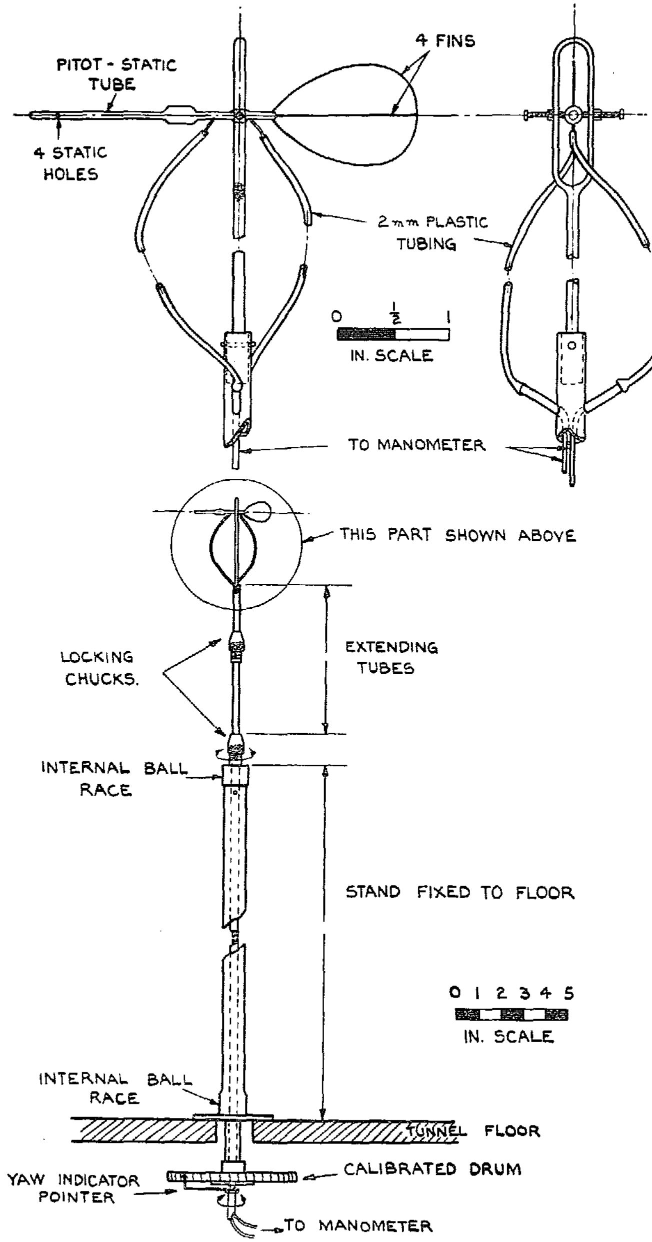

FIG. 3. General assembly of traverse instrument.

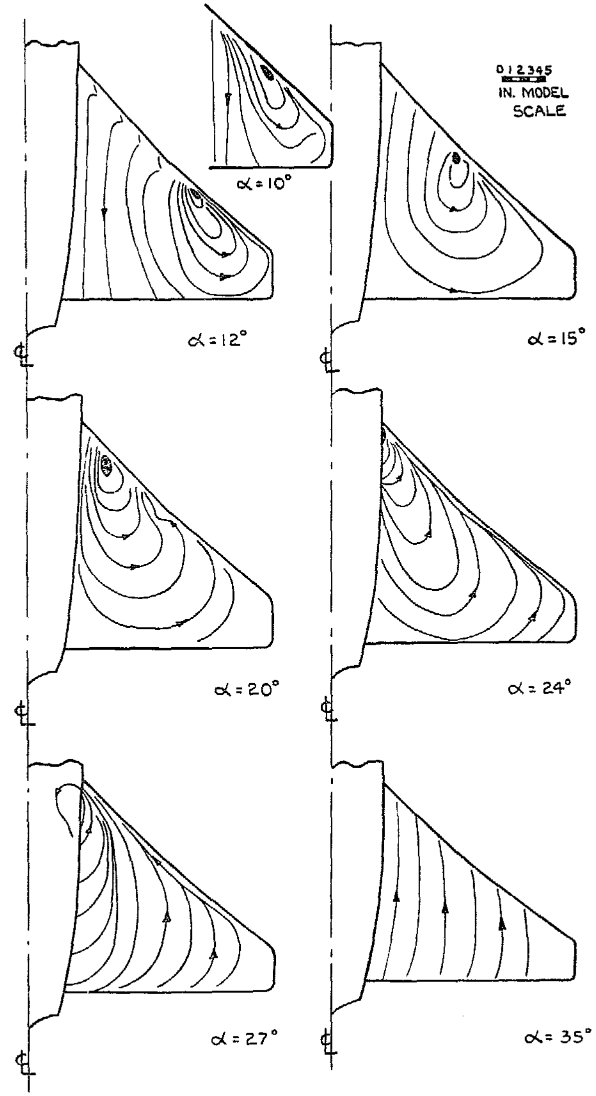

FIG. 4. Plan view of flow in the boundary layer on the upper surface of the delta wing.

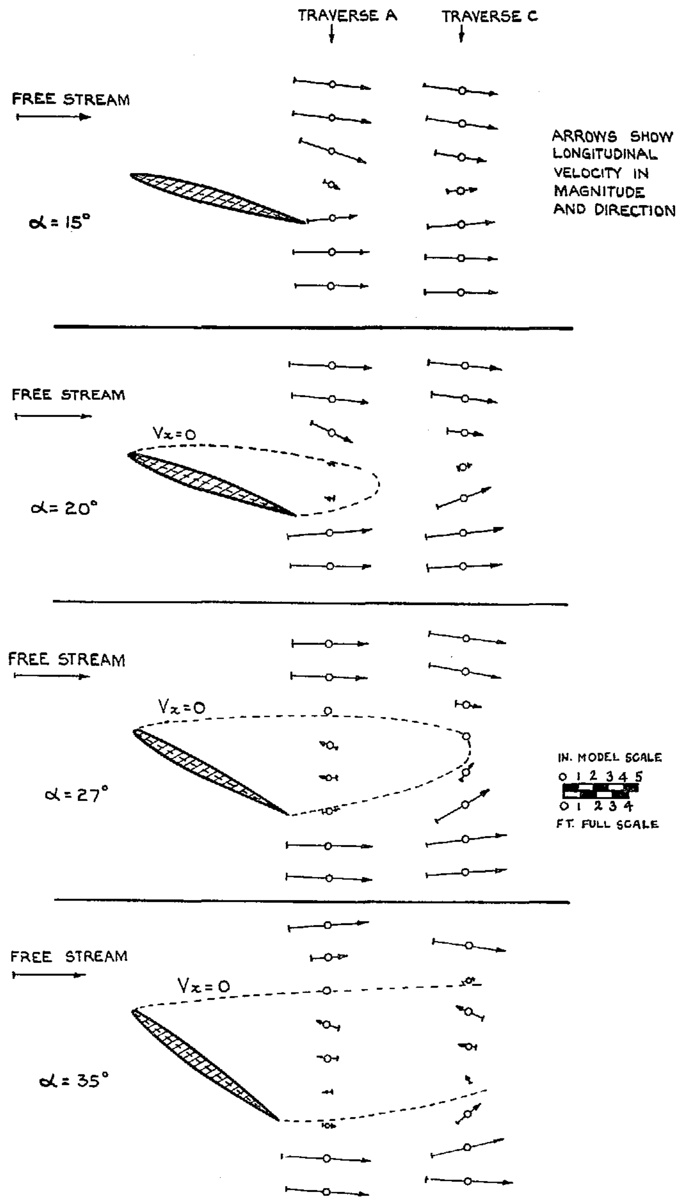

FIG. 7. Velocity in the x-z plane at 0·75 semi-span of the delta wing (Traverses A and C).

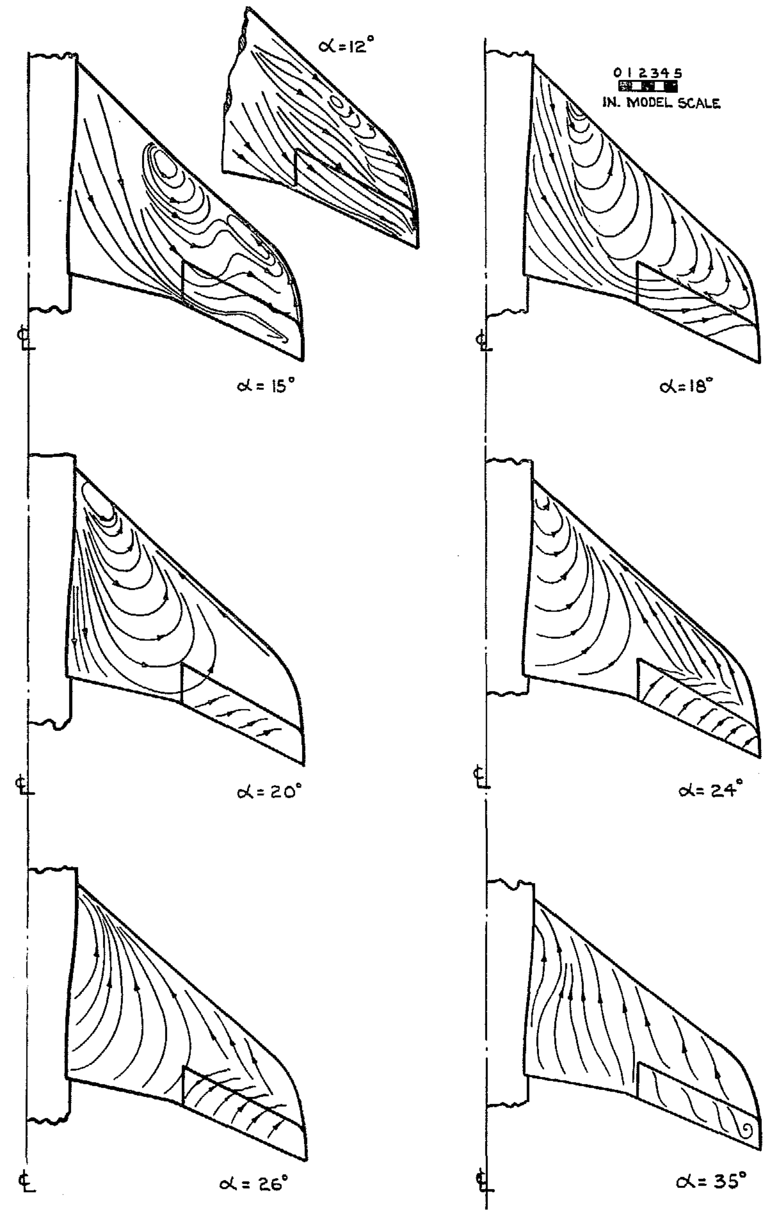

FIG. 8. Plan view of flow in the boundary layer on the upper surface of the 40-deg swept wing.

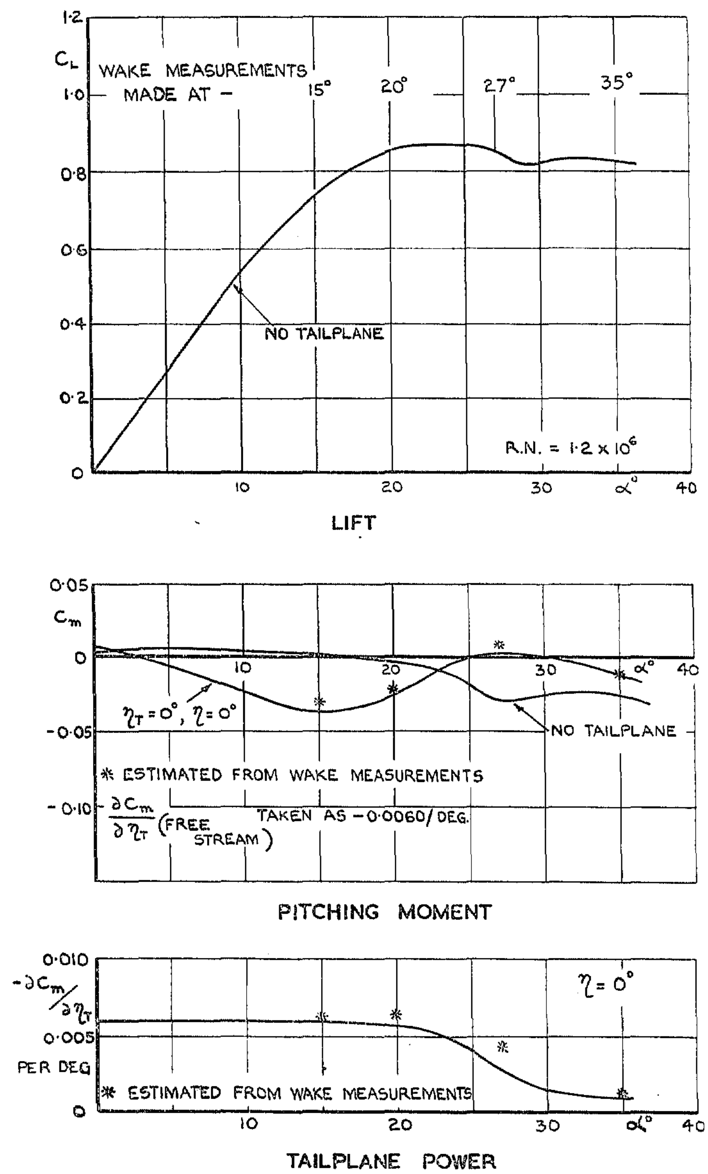

FIG. 10. Balance measurements on *Javelin* (Flaps 0 deg).

(42557) Wt. 52 K7 1/58 F.M. & S.

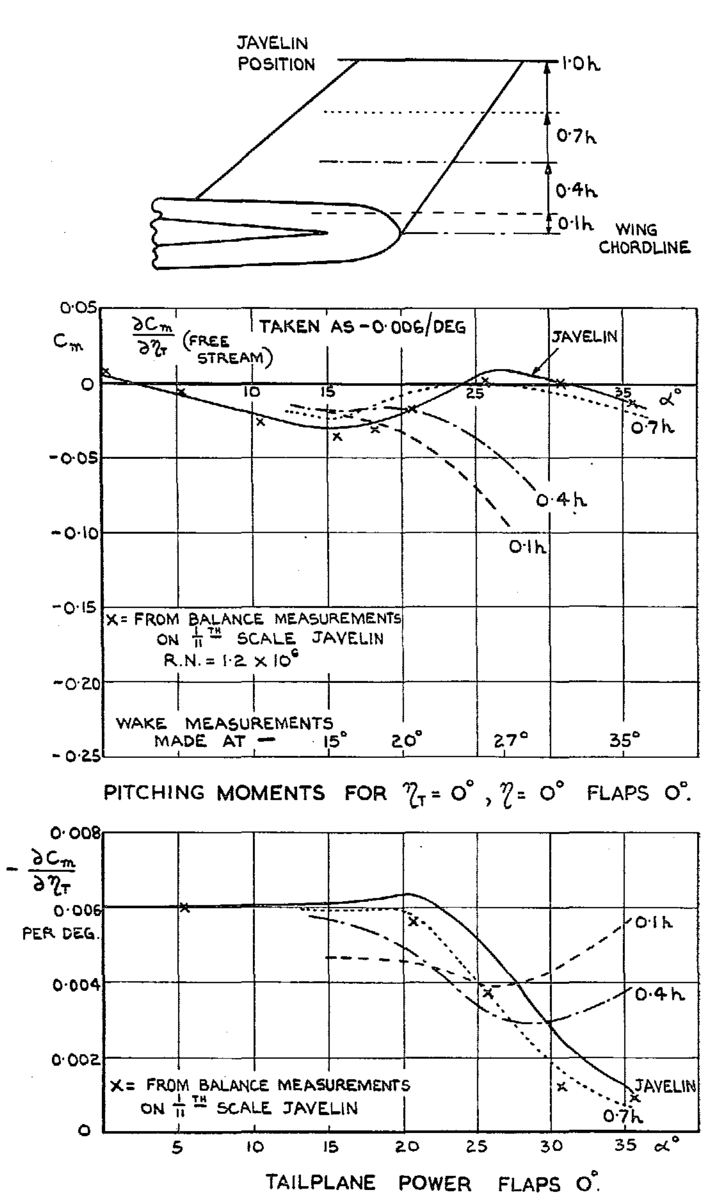

FIG. 11. Effect of tailplane height on the pitching moment of the delta model.

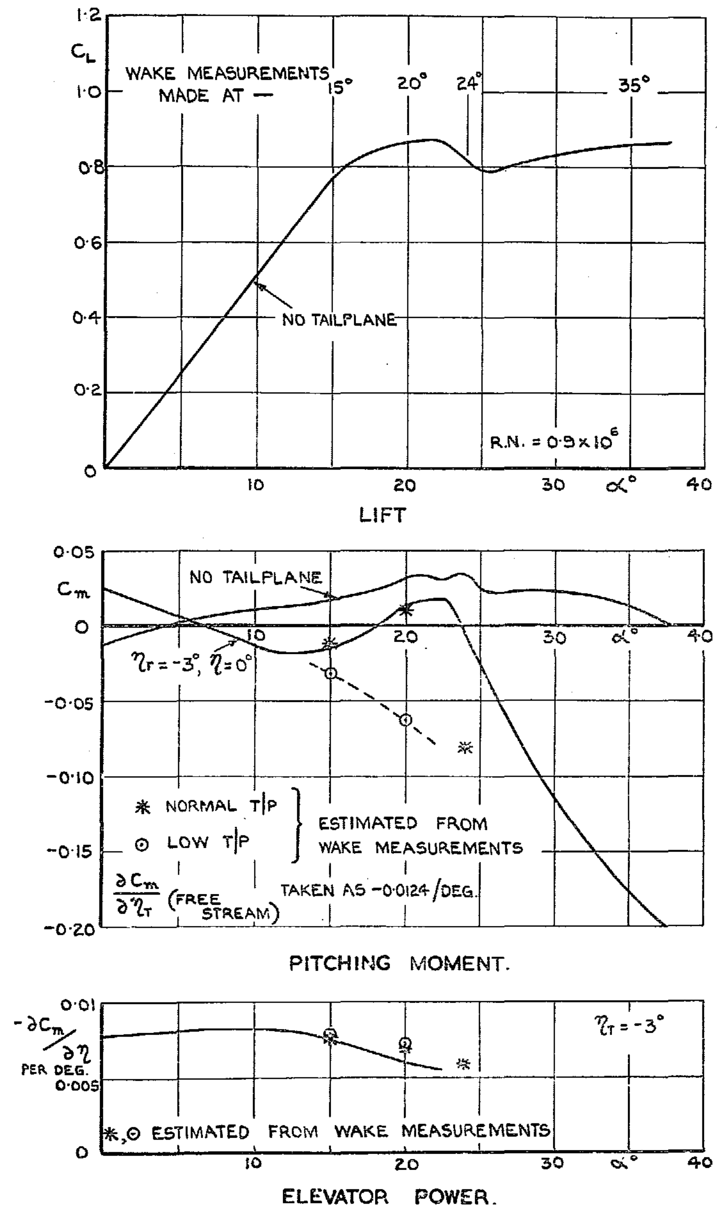

FIG. 12. Balance measurements on *Swift* without fences (Flaps 0 deg).

PRINTED IN GREAT BRITAIN

Publication of the Aeronautical Research Council

ANNUAL TECHNICAL REPORTS OF THE AERONAUTICAL RESEARCH COUNCIL (BOUND VOLUMES)

1939 Vol. I. Aerodynamics General, Performance, Airscrews, Engines. 50*s.* (52*s.*)
Vol. II. Stability and Control, Flutter and Vibration, Instruments, Structures, Seaplanes, etc. 63*s.* (65*s.*)

1940 Aero and Hydrodynamics, Aerofoils, Airscrews, Engines, Flutter, Icing, Stability and Control Structures, and a miscellaneous section. 50*s.* (52*s.*)

1941 Aero and Hydrodynamics, Aerofoils, Airscrews, Engines, Flutter, Stability and Control Structures. 63*s.* (65*s.*)

1942 Vol. I. Aero and Hydrodynamics, Aerofoils, Airscrews, Engines. 75*s.* (77*s.*)
Vol. II. Noise, Parachutes, Stability and Control, Structures, Vibration, Wind Tunnels. 47*s.* 6*d.* (49*s.* 6*d.*)

1943 Vol. I. Aerodynamics, Aerofoils, Airscrews. 80*s.* (82*s.*)
Vol. II. Engines, Flutter, Materials, Parachutes, Performance, Stability and Control, Structures. 90*s.* (92*s.* 9*d.*)

1944 Vol. I. Aero and Hydrodynamics, Aerofoils, Aircraft, Airscrews, Controls. 84*s.* (86*s.* 6*d.*)
Vol. II. Flutter and Vibration, Materials, Miscellaneous, Navigation, Parachutes, Performance, Plates and Panels, Stability, Structures, Test Equipment, Wind Tunnels. 84*s.* (86*s.* 6*d.*)

1945 Vol. I. Aero and Hydrodynamics, Aerofoils. 130*s.* (132*s.* 9*d.*)
Vol. II. Aircraft, Airscrews, Controls. 130*s.* (132*s.* 9*d.*)
Vol. III. Flutter and Vibration, Instruments, Miscellaneous, Parachutes, Plates and Panels, Propulsion. 130*s.* (132*s.* 6*d.*)
Vol. IV. Stability, Structures, Wind Tunnels, Wind Tunnel Technique. 130*s.* (132*s.* 6*d.*)

Annual Reports of the Aeronautical Research Council—

1937 2*s.* (2*s.* 2*d.*) 1938 1*s.* 6*d.* (1*s.* 8*d.*) 1939–48 3*s.* (3*s.* 5*d.*)

Index to all Reports and Memoranda published in the Annual Technical Reports, and separately—

April, 1950 - - - - R. & M. 2600 2*s.* 6*d.* (2*s.* 10*d.*)

Author Index to all Reports and Memoranda of the Aeronautical Research Council—

1909—January, 1954 R. & M. No. 2570 15*s.* (15*s.* 8*d.*)

Indexes to the Technical Reports of the Aeronautical Research Council—

December 1, 1936—June 30, 1939	R. & M. No. 1850	1*s.* 3*d.* (1*s.* 5*d.*)
July 1, 1939–June 30, 1945	R. & M. No. 1950	1*s.* (1*s.* 2*d.*)
July 1, 1945—June 30, 1946	R. & M. No. 2050	1*s.* (1*s.* 2*d.*)
July 1, 1946—December 31, 1946	R. & M. No. 2150	1*s.* 3*d.* (1*s.* 5*d.*)
January 1, 1947—June 30, 1947	R. & M. No. 2250	1*s.* 3*d.* (1*s.* 5*d.*)

Published Reports and Memoranda of the Aeronautical Research Council—

Between Nos. 2251–2349	R. & M. No. 2350	1*s.* 9*d.* (1*s.* 11*d.*)
Between Nos. 2351–2449	R. & M. No. 2450	2*s.* (2*s.* 2*d.*)
Between Nos. 2451–2549	R. & M. No. 2550	2*s.* 6*d.* (2*s.* 10*d.*)
Between Nos. 2551–2649	R. & M. No. 2650	2*s.* 6*d.* (2*s.* 10*d.*)
Between Nos. 2651–2749	R. & M. No. 2750	2*s.* 6*d.* (2*s.* 10*d.*)

Prices in brackets include postage

HER MAJESTY'S STATIONERY OFFICE

York House, Kingsway, London W.C.2; 423 Oxford Street, London W.1; 13a Castle Street, Edinburgh 2; 39 King Street, Manchester 2; 2 Edmund Street, Birmingham 3; 109 St. Mary Street, Cardiff; Tower Lane, Bristol, 1; 80 Chichester Street, Belfast, *or through any bookseller.*

S.O. Code No. 23-3078

R. & M. No. 3078